J. Fluid Mech. (1990), *vol.* 221, *pp.* 597–611
Printed in Great Britain

Numerical study of elliptical modons using a spectral method

By JOHN P. BOYD AND HONG MA

Department of Atmospheric, Oceanic and Space Sciences, and Laboratory for Scientific Computation, University of Michigan, 2455 Hayward Avenue, Ann Arbor MI 48109, USA

(Received 10 July 1989 and in revised form 11 May 1990)

We study the relationship between dynamical structure and shape for vortex pairs, now usually named 'modons'. When the boundary between the exterior irrotational flow and the inner core of non-zero vorticity is a circle, an analytical solution is known. Here, we generalize the circular modons to solitary vortex pairs whose vorticity boundary is an ellipse. We find that as the eccentricity of the ellipse increases, the vorticity becomes concentrated in narrow ridges which run just inside the elliptical vorticity boundary and continue just inside the line of zero vorticity which divides the two vortices. Each vortex becomes increasingly 'hollow' in the sense that each contains a broad valley of low vorticity which is completely enclosed by the ridge of high vorticity already described. The relationship between vorticity ζ and streak function Ψ, which is linear for the circular modons, becomes strongly nonlinear for highly eccentric modons, qualitatively resembling $\zeta \propto \Psi e^{-\lambda\Psi}$ for some constant λ. In this study, we neglect the Earth's rotation, but our method is directly applicable to quasi-geostrophic modons, too. An efficient and simple spectral method for modon problems is provided.

1. Introduction

'Modon' is a generally used name for a solitary pair of contra-rotating vortices. *Hydrodynamics* (Lamb 1932) is probably the earliest description of modons although the term 'modon' was invented by Stern (1975). In the past three decades, modons have aroused great research interest especially in geophysics and plasma physics (see table 1). The main reason for this enthusiasm for modon study is that vortices and vortex pairs are fundamental parts of the geofluid environment, i.e. the atmosphere and ocean. A thorough modon theory will greatly help to understand, explain, and predict many important atmospheric and oceanic phenomena such as atmospheric blocking and Gulf Stream rings.

The existing modon solutions can be divided into two categories: exact analytical solutions and numerical approximations. There are some common assumptions among the analytical models inherited from Lamb's original model. These common assumptions are that the boundary between the rotational and irrotational (without β effect) flow is a circle; the vorticity is a linear function of the stream function; the tangential velocity is continuous everywhere. The mathematical problem is greatly simplified by these assumptions so that exact analytical modon solutions are possible. In spherical geometry, these solutions are associated Legendre functions; in Cartesian geometry, these circular modons are Bessel functions.

In the numerical category, time integration has been used to study the process of modon formation from the collision of monopoles (McWilliams 1983); to test the

Modon models	Modon shapes	$\zeta = F(\Psi)$	Mathematical approaches	Spherical effects
Lamb 1932	circle	linear	analytical	no
Batchelor 1967	circle	linear	analytical	no
Stern 1975	circle	linear	analytical	β plane approx.
Larichev & Reznik 1976	circle	linear	analytical	β plane approx.
Flierl *et al.* 1980, 1983	circle	linear	analytical/finite difference	β plane approx.
McWilliams 1980, 1983; McWilliams *et al.* 1981	circle	linear	analytical/finite difference	β plane approx.
Shen 1981	arbitrary	unspecified	integral constraint theorems	β plane approx.
Tribbia 1984	circle	linear	analytical	spherical coordinates
Verkley 1984, 1987	circle/ calculated	linear/ calculated	analytical/inverse power/spherical harmonics	spherical coordinates
Deem & Zabusky 1978	calculated*	$\zeta = \text{const}$	contour dynamics/ relaxation	no
Pierrehumbert 1980	calculated	$\zeta = \text{const}$	contour dynamics	no
Tanveer 1986	calculated	$\zeta = \text{const}$	conformal mapping	no
Eydeland & Turkington 1988	calculated	$\zeta = \Psi^{r-1}$	variational method	no
Present work	ellipse	calculated	Chebyshev pseudospectral/ Newton's iteration	no

* This quantity is determined by solutions of the model rather than by being specified *a priori*.

TABLE 1. Some characteristics of modon models

stability of modons (McWilliams *et al.* 1981); and to investigate other modon interaction processes (McWilliams & Zabusky 1982; Larichev & Reznik 1983). Other numerical studies including this work have computed modons directly by solving a nonlinear boundary-value problem to relax the restriction of a circular vorticity boundary.

There are some concerns about the analytical solutions because modons observed in nature are often not circular, in the sense that the boundary between the rotational and irrotational flow is not an exact circle, and the linear relationship between vorticity and stream function which is assumed by the analytical theories is not generally true for non-circular modons. It is necessary to have modon models to deal with these aspects. The numerical models have showed various modon shapes and nonlinear relationships between vorticity and stream function (Deem & Zabusky 1978; Tanveer 1986; Verkley 1987; Eydeland & Turkington 1988; and the present work).

The shape of the modon and the relationship between the vorticity and the stream function, i.e. $\zeta = F(\Psi)$, are two factors which can be used to determine the modon solutions, and only one of them is independent. All except us have specified the function $F(\Psi)$ which is the vorticity; the vorticity boundary is then calculated as part of the numerical solution. In contrast, we specify the vorticity boundary to be an ellipse and compute $F(\Psi)$.

The computational advantage of our approach is that it allows us to split the domain into two so that the solution is smooth and analytic everywhere within each subdomain. The vorticity has a discontinuous slope at the vorticity boundary which would destroy the exponential accuracy of the spectral method if we attempted to use a single Chebyshev–Fourier series over the whole flow.

The present paper uses a spectral method to compute elliptical modons. The features of this model are: (i) The shape of the modon can be changed continuously from a circle to a very narrow ellipse through adjusting one parameter which enables us to compare the behaviour of modons at different shapes rather easily; (ii) The modon is computed in a frame of reference moving with the vortex pair (the modon is stationary in this moving coordinate system); (iii) The exterior flow is irrotational; (iv) The modon is computed by solving a third-order nonlinear partial differential equation. Two boundary conditions are that the streak function and its first derivative are continuous at the boundary. The third boundary condition is that of boundedness at the origin; (v) The relation between the vorticity and the stream function of the interior flow is single valued but nonlinear.

The numerical techniques employed are Chebyshev polynomials and Fourier series in elliptical coordinates, and the Newton–Kantorovich iteration. These methods are so efficient for the present modon problem that even a micro-computer can handle the computation.

2. Mathematical formulation

2.1. *Governing equation*

For steady, frictionless, barotropic flow, if we assume the coordinate system is moving in the x-direction with speed c, then the vorticity equation can be written as

$$\nabla(\psi + cy) \times \nabla\zeta = 0, \tag{2.1}$$

where ψ is stream function, ζ is vorticity. If we use the notation of the 'streak function' Ψ, which was introduced by Flierl *et al.* (1980), then (2.1) can be written as

$$\nabla\Psi \times \nabla\zeta = 0, \tag{2.2}$$

where the streak function is

$$\Psi \equiv \psi + cy. \tag{2.3}$$

2.2. *Transformation and analysis under elliptical coordinates*

Let

$$x = d\cosh(\xi)\cos(\eta), \tag{2.4}$$

$$y = d\sinh(\xi)\sin(\eta), \tag{2.5}$$

where d is half of the distance between the foci (figure 1).

Under elliptical coordinates (ξ, η) the governing equation (2.2) becomes

$$1/[d^2(\cosh^2(\xi) - \cos^2(\eta))]\left(\frac{\partial\Psi}{\partial\xi}, \frac{\partial\Psi}{\partial\eta}\right) \times \left(\frac{\partial\zeta}{\partial\xi}, \frac{\partial\zeta}{\partial\eta}\right) = 0, \tag{2.6}$$

where the vorticity ζ is

$$\zeta = \nabla^2\Psi = 1/[d^2(\cosh^2(\xi) - \cos^2(\eta))]\,(\Psi_{\xi\xi} + \Psi_{\eta\eta}). \tag{2.7}$$

Substituting (2.7) into (2.6) and multiplying through by a factor, we obtain

$$\begin{aligned}\Psi_\xi \Psi_{\xi\xi\eta} + \Psi_\xi \Psi_{\eta\eta\eta} - \{2\cos(\eta)\sin(\eta)/[\cosh^2(\xi) - \cos^2(\eta)]\}\,(\Psi_\xi \Psi_{\xi\xi} \\ + \Psi_\xi \Psi_{\eta\eta}) - \Psi_\eta \Psi_{\xi\xi\xi} - \Psi_\eta \Psi_{\xi\eta\eta} + \{2\cosh(\xi)\sinh(\xi)/[\cosh^2(\xi) \\ - \cos^2(\eta)]\}\,(\Psi_\eta \Psi_{\xi\xi} + \Psi_\eta \Psi_{\eta\eta}) = 0.\end{aligned} \tag{2.8}$$

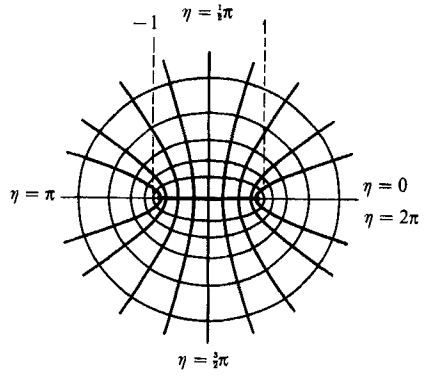

FIGURE 1. Elliptical coordinates. The ellipses are contours of constant ξ; the hyperbolas are contours of constant η where η is the angular coordinate.

If we assume that the boundary between the interior and exterior flow is the ellipse, $\xi = \xi_0$, and that the streak function Ψ and its first derivative are continuous at the boundary, and, without losing generality, that $\Psi = 0$ at $\xi = \xi_0$, then the irrotational exterior flow has the solution

$$\Psi = cd \sin(\eta)\,[\sinh(\xi) - \sinh(\xi_0)\exp(\xi_0 - \xi)], \tag{2.9}$$

when the exterior flow at infinity is parallel to the major axis of the ellipse $\xi = \xi_0$. This exterior solution (2.9) is the same as the solution for the problem of the stream past a solid elliptical body (Lamb 1932).

Observe that every term in (2.8) is quadratically nonlinear. This implies that if $\Psi(\xi, \eta)$ is a solution of (2.8), then $\lambda\Psi(\xi, \eta)$ is also a solution for any constant λ. The exterior solution is directly proportional to c. It follows that if we have a solution that satisfies the differential equation and boundary condition for $c = c_0$, then $\lambda\Psi(\xi, \eta)$ is a solution for $c = \lambda c_0$ if the boundary ellipse is unchanged. Thus, the phase speed c merely provides the amplitude for the solution. The shape of the modon is independent of c.

Similarly, (2.8) is also independent of d, the constant that appears in the definition of the elliptical coordinates (2.4) and (2.5). Noting that the exterior solution is proportional to d, we find that the shape of the modon is also independent of d except that d stretches the width of the solution in both x and y. Thus, the only non-trivial parameter is ξ_0, the quasi-radial coordinate of the ellipse bounding the interior rotational region.

It follows that it is only necessary to solve the elliptical modon problem for $c = 1$ and $d = 1$; all other modons with that value of ξ_0 can be obtained from the ($c = d = 1$) solution by rescaling the amplitude and the spatial coordinates.

3. Numerical methods for the interior solution

Since (2.8) is nonlinear, we solve it via Newton–Kantorovich iteration.

Let $$\Psi^{i+1} = \Psi^i + \Delta^i, \tag{3.1}$$

where Ψ is the value of interior streak function at the ith iteration, and Δ^i is the correction to Ψ^i.

Substituting (3.1) into (2.8) and neglecting all nonlinear terms of Δ^i, the linearized equation for Δ^i is

$$\begin{aligned}\Delta^i_\xi \Psi^i_{\xi\xi\eta} + \Psi^i_\xi \Delta^i_{\xi\xi\eta} + \Psi^i_\xi \Delta^i_{\eta\eta\eta} + \Delta^i_\xi \Psi^i_{\eta\eta\eta} - A(\Delta^i_\xi \Psi i_{\xi\xi} + \Psi^i_\xi \Delta^i_{\xi\xi} + \Delta^i_\xi \Psi^i_{\eta\eta} \\ + \Psi^i_\xi \Delta^i_{\eta\eta}) - \Delta^i_\eta \Psi^i_{\xi\xi\xi} - \Psi^i_\eta \Delta^i_{\xi\xi\xi} - \Delta^i_\eta \Psi^i_{\xi\eta\eta} - \Psi^i_\xi \Delta^i_{\xi\eta\eta} + B(\Delta^i_\eta \Psi^i_{\xi\xi} \\ + \Psi^i_\eta \Delta^i_{\xi\xi} + \Delta^i_\eta \Psi^i_{\eta\eta} + \Psi^i_\eta \Delta^i_{\eta\eta}) = -\Psi^i_\xi \Psi^i_{\xi\xi\eta} - \Psi^i_\xi \Psi^i_{\eta\eta\eta} + A(\Psi^i_\xi \Psi^i_{\xi\xi} \\ + \Psi^i_\xi \Psi^i_{\eta\eta}) + \Psi^i_\eta \Psi^i_{\xi\xi\xi} + \Psi^i_\eta \Psi^i_{\xi\eta\eta} - B(\Psi^i_\eta \Psi^i_{\xi\xi} + \Psi^i_\eta \Psi^i_{\eta\eta}),\end{aligned} \tag{3.2}$$

where $$A = \frac{2\cos(\eta)\sin(\eta)}{\cosh^2(\xi) - \cos^2(\eta)}, \quad B = \frac{2\cosh(\xi)\sinh(\xi)}{\cosh^2(\xi) - \cos^2(\eta)}.$$

From (2.9), we know the exterior streak function is zero at $\xi = \xi_0$, but not its first derivative. Since we require the first derivative as well as the streak function to be continuous at the boundary $\xi = \xi_0$, we should impose the same boundary values for the interior solution. It is convenient to write

$$\Psi = P + V, \tag{3.3}$$

where P is a known function of ξ and η that satisfies the inhomogeneous boundary condition of matching the first derivative of the exterior solution (2.9):

$$P(\xi, \eta) = cd \exp(\xi_0)\, \xi_0 \sin(\eta)/2\left(-\left(\frac{\xi}{\xi_0}\right) + \left(\frac{\xi}{\xi_0}\right)^3\right). \tag{3.4}$$

Now the problem of calculating Ψ becomes that of calculating $V(\xi, \eta)$ which satisfies two homogeneous boundary conditions:

$$V(\xi, \eta) = 0 \quad \text{at } \xi = \xi_0, \tag{3.5}$$

$$\frac{\partial V(\xi, \eta)}{\partial \xi} = 0 \quad \text{at } \xi = \xi_0, \tag{3.6}$$

plus the implicit condition of boundedness as $\xi \to 0$.

If we let $$\Psi^0 = P(\xi, \eta), \tag{3.7}$$

then compare (3.1) with (3.4) we know

$$\Psi^i(\xi, \eta) = P(\xi, \eta) + \sum_{n=0}^{i-1} \Delta^n(\xi, \eta), \tag{3.8}$$

$$V(\xi, \eta) = \sum_{i=0}^{N} \Delta^i(\xi, \eta). \tag{3.9}$$

Obviously, $\Delta^i(\xi, \eta)$ should satisfy the homogeneous boundary conditions

$$\Delta^i(\xi, \eta) = 0 \quad \text{at } \xi = \xi_0, \tag{3.10}$$

$$\frac{\partial \Delta^i(\xi, \eta)}{\partial \xi} = 0 \quad \text{at } \xi = \xi_0. \tag{3.11}$$

Equation (3.2) plus the boundary conditions (3.10) and (3.11) constitute a linear system, which is going to be solved by the spectral method. The streak function has the following properties:

(i) streak-function Ψ and its first derivative $\partial\Psi/\partial\xi$ are continuous and Ψ itself equals zero at boundary $\xi = \xi_0$.

(ii) Ψ is periodic in η.

(iii) Ψ is antisymmetric about $\eta = 0$ and symmetric about $\eta = \frac{1}{2}\pi$.

The symmetry properties follow from those of the analytical, circular modon and the fact that changing the shape at the vorticity boundary to an ellipse does not disrupt those symmetries. The periodicity in η implies that a Fourier basis is best for this coordinate. We use Chebyshev polynomials for the non-periodic coordinate ξ. We can greatly improve the efficiency of the spectral method by restricting the basis to functions that have the same symmetries as Ψ. This implies

$$\Delta^i = \sum_{n=1}^{n_1} \sum_{m=1}^{n_2} a_{mn} \sin[(2m-1)\eta]\, \phi_{2n+3}(\xi). \tag{3.12}$$

The basis function ϕ_{2n+3} is defined as

$$\phi_{2n+3}(\xi) = \phi_{2n+3}(\xi_0 \cos(t)) = T_{2n+3}(t) + \alpha_{2n+3}\, T_1(t) + \beta_{2n+3}\, T_3(t), \tag{3.13}$$

where $T_n(t)$ is the Chebyshev basis function of nth order defined as $T_n(\cos(t)) \equiv \cos(nt)$.

α, β are chosen as

$$\alpha_{2n+3} = \tfrac{1}{8}[(2n+3)^2 - 1] - 1 \tag{3.14}$$

$$\beta_{2n+3} = \tfrac{1}{8}[1 - (2n+3)^2] \tag{3.15}$$

so that boundary conditions (3.10) and (3.11) are satisfied. This special technique is called 'basis recombination' (Boyd 1989). With such recombined basis functions, every basis function individually satisfies the homogeneous boundary conditions.

Substituting (3.12) into (3.2), we obtain:

$$\begin{aligned}
&\sum_{m=1}^{n_1} \sum_{n=1}^{n_2} a_{mn} \{ \phi'_{2n+3} \sin[(2m-1)\eta]\, \Psi^i_{\xi\xi\eta} \\
&\quad + (2m-1)\, \phi''_{2n+3}(\xi) \cos[(2m-1)\eta]\, \Psi^i_{\xi} - (2m-1)^3 \phi_{2m+3}(\xi) \cos[(2m-1)\eta]\, \Psi^i_{\xi}, \\
&\quad + \phi'_{2n+3}(\xi) \sin[(2m-1)\eta]\, \Psi^i_{\eta\eta\eta} - A[\phi'_{2n+3}(\xi) \sin[(2m-1)\eta]\, \Psi^i_{\xi\xi} \\
&\quad + \phi''_{2n+3}(\xi) \sin(2m-1)\, \Psi^i_{\xi} + \phi'_{2n+3}(\xi) \sin[(2m-1)\eta]\, \Psi^i_{\eta\eta} \\
&\quad - (2m-1)^2 \phi_{2n+3}(\xi) \sin[(2m-1)\eta]\, \Psi^i_{\xi}] \\
&\quad - (2m-1)\, \phi_{2n+3}(\xi) \cos[(2m-1)\eta]\, \Psi^i_{\xi\xi\xi} - \phi'''_{2n+3}(\xi) \sin[(2m-1)\eta]\, \Psi^i_{\eta} \\
&\quad - (2m-1)\, \phi_{2n+3}(\xi) \cos[(2m-1)\eta]\, \Psi^i_{\xi\eta\eta} + (2m-1)^2 \phi'_{2n+3}(\xi) \sin[(2m-1)\eta]\, \Psi^i_{\eta} \\
&\quad + B[(2m-1)\, \phi_{2n+3}(\xi) \cos[(2m-1)\eta]\, \Phi^i_{\xi\xi} \\
&\quad + \phi''_{2n+3}(\xi) \sin[(2m-1)\eta]\, \Psi^i_{\eta} + (2m-1)\, \phi_{2n+3}(\xi) \cos[(2m-1)\eta]\, \Psi^i_{\eta\eta} \\
&\quad - (2m-1)^2 \phi_{2n+3}(\xi) \sin[(2m-1)\eta]\, \Psi^i_{\eta}] \} = -\Psi^i_{\xi} \Psi^i_{\xi\xi\eta} - \Psi^i_{\xi} \Psi^i_{\eta\eta\eta} + A(\Psi^i_{\xi} \Psi^i_{\xi\xi} \\
&\quad + \Psi^i_{\xi} \Psi^i_{\eta\eta}) + \Psi^i_{\eta} \Psi^i_{\xi\xi\xi} + \Psi^i_{\eta} \Psi^i_{\xi\eta\eta} - B(\Psi^i_{\eta} \Psi^i_{\xi\xi} + \Psi^i_{\eta} \Psi^i_{\eta\eta})
\end{aligned} \tag{3.16}$$

where $\phi'_{2n+3}(\xi)$, $\phi''_{2n+3}(\xi)$, $\phi'''_{2n+3}(\xi)$ are the first-, second-, and third-order derivatives of $\phi_{2n+3}(\xi)$. The calculation of Ψ^i and its derivatives is carried out following (3.8).

Equation (3.16) contains $n_1 \times n_2$ unknown coefficients a_{mn}. In order to obtain $n_1 \times n_2$ equations we apply the pseudospectral method, i.e. apply (3.16) at $n_1 \times n_2$ interpolation points in (ξ, η)-space. There are n_1 evenly spaced interpolation points in the spectral space t ranging from 0 to $\frac{1}{2}\pi$, which corresponds to an unevenly spaced interpolation in the physical space ξ ranging from ξ_0 to 0. There are n_2 evenly spaced interpolation points in physical space η ranging from 0 to $\frac{1}{2}\pi$. We only calculate the

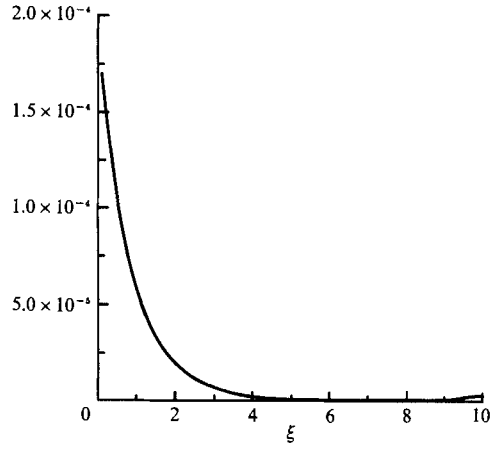

FIGURE 2. The rescaled absolute error of streak function between Lamb's analytical circular modon solution and the spectral numerical solution for elliptical modon with $\xi_0 = 10.0$ in which case the difference between the major axis and minor axis of the modon boundary ellipse is less than 10^{-4}. The error has been rescaled by dividing it by the maximum of the stream function. The streak function values are taken along $\eta = \frac{1}{2}\pi$.

ξ_0	n_1	n_2	Truncation error	Iteration times	cpu time*
10	50	1	10^{-5}	16	26 s
3	30	2	10^{-5}	6	22 s
1	25	8	10^{-6}	4	3 min 10 s
0.5	41	14	10^{-6}	5	23 min 56 s

* Computing times are for a single processer on an Alliant FX80, superminicomputer.

TABLE 2. Numerical factors for experiments

solution for η values between 0 and $\frac{1}{2}\pi$ because the solution for η between $\frac{1}{2}\pi$ and 2π can be deduced by the symmetry properties of Ψ. In this way we have saved a lot of computation time and storage space. Now the remaining problem is only a matter of linear algebra. Since in most cases $n_1 \times n_2$ is much smaller than 1000, Gaussian elimination is very efficient even with a microcomputer. This is one of the major virtues of the spectral method over finite difference. For the same problem and same precision, finite differences algorithms usually require a matrix much larger than that of the spectral method.

4. Numerical results

We have run a series of numerical experiments with different values of ξ_0. The larger ξ_0 is, the closer the shape of the modon is to a circle. $\xi_0 = 10$ is so close to a circle that the difference between the major axis and minor axis is less than 10^{-4}. The difference between the numerical solution of $\xi_0 = 10$ and the Lamb–Batchelor analytical solution is given in figure 2, which shows that for a large value of ξ_0 the numerical solution is almost identical to Lamb–Batchelor's analytical solution. Table 2 gives several basic numerical factors for these experiments. Figures 3(*a*)–3(*f*) are the contour plots of streak function and vorticity for different values of ξ_0.

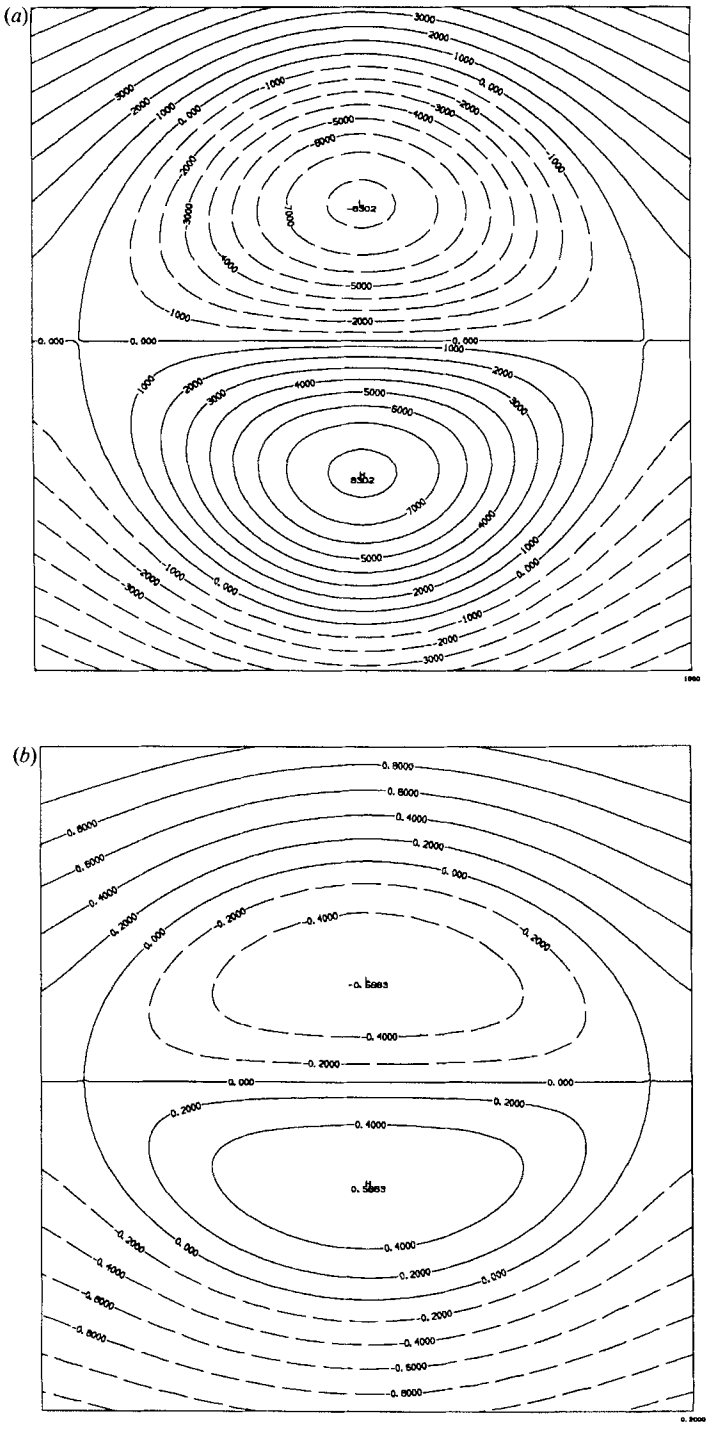

FIGURE 3(a, b). For caption see page 606.

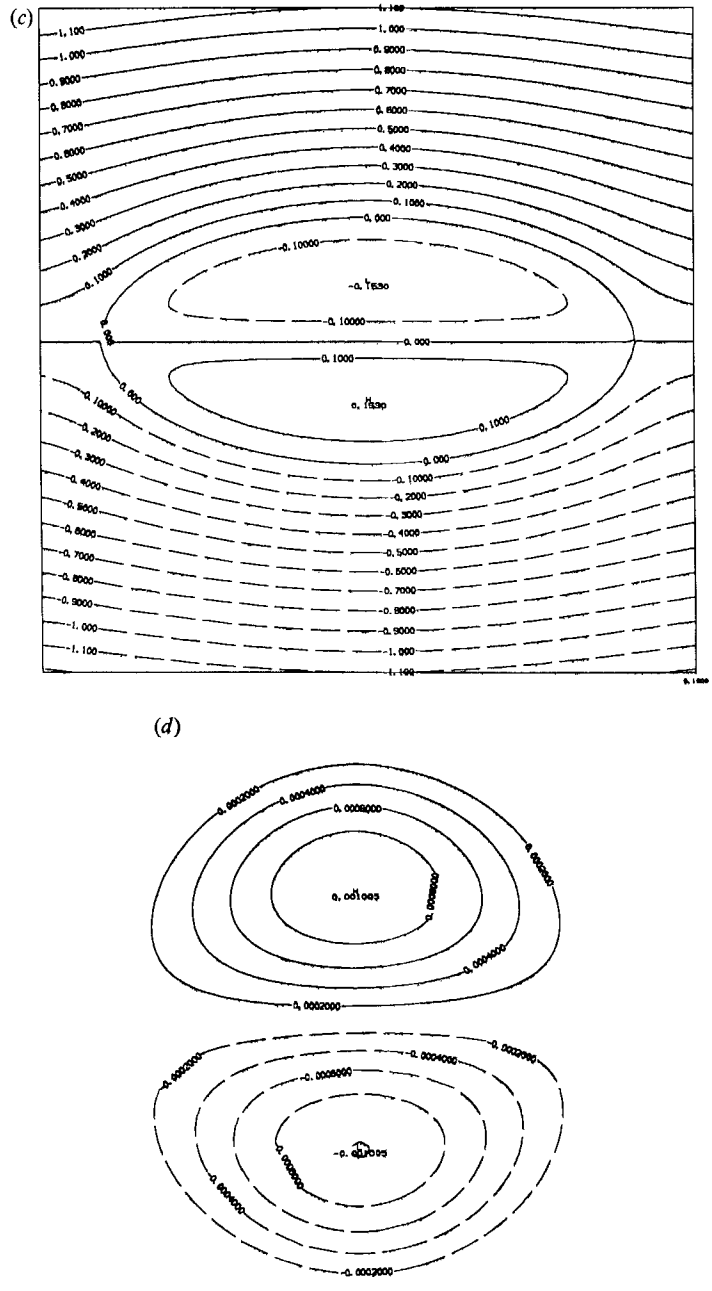

FIGURE 3(*c*,*d*). For caption see next page.

For the circular modon, the vorticity variation within the vortex is very homogeneous and the vorticity maximum is at the centre of each vortex (figure 3*d*). However, this is not true for elliptical modons. When the ellipticity is large, there is a strong vorticity shear region at the boundary between the rotational flow and irrotational flow (figure 4), and unlike the circular modon case the maximum vorticity does not locate at the centre of the vortex but near its boundary. Both the maximum vorticity and the vorticity shear at the boundary grow stronger as the value of ξ_0 becomes smaller, i.e.

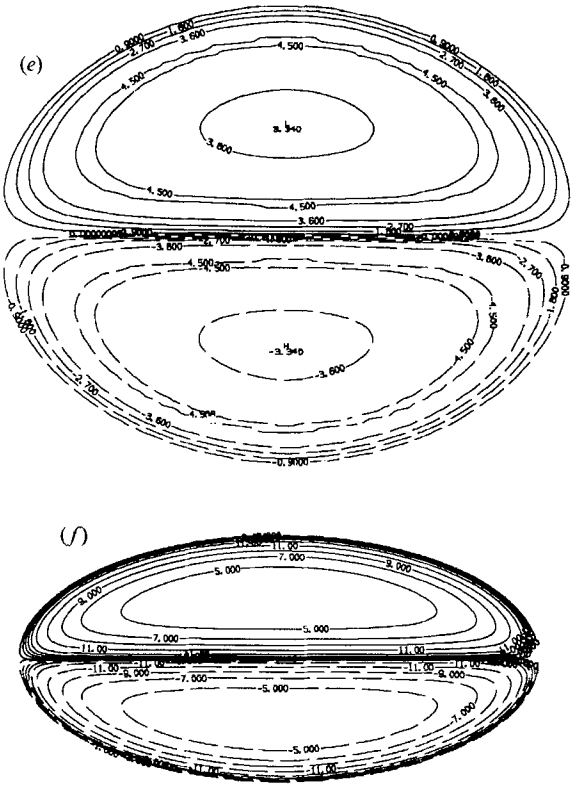

FIGURE 3. Contour plots of the streak function and vorticity. (*a*) The contour plot of streak function for $\xi_0 = 10.0$. (*b*) The contour plot of streak function for $\xi_0 = 1.0$. (*c*) The contour plot of streak function for $\xi_0 = 0.5$. (*d*) The contour plot of vorticity for $\xi_0 = 10.0$. (*e*) The contour plot of vorticity for $\xi_0 = 1.0$. (*f*) The contour plot of vorticity for $\xi_0 = 0.5$.

the boundary ellipse becomes more eccentric (figure 3*e*, *f*). For $\xi_0 = 1.0$ and 0.5, the ratio between the major axis and the minor axis of the boundary ellipse is 1.31 and 2.16 respectively. Figure 5 describes the relation between streak function and vorticity for circular modons and elliptical modons. For circular modons (figure 5*a*) the relationship between streak function and vorticity is linear, and the vortex is much weaker than in the elliptical modons, even though the exterior flow speed at infinity (which is also the modon phase speed) is the same in all figures. The relationship between the streak function and vorticity is nonlinear for elliptical modons. When the eccentricity of the boundary ellipse increases, the peak in the scatter plots of vorticity versus streak function becomes sharper and the maximum vorticity becomes larger (figure 5*b*, *c*).

The gradient of vorticity near the elliptical boundary becomes sharper as ξ_0 becomes smaller, which means higher resolution is needed. Theoretically, it is possible for us to calculate the modon solution with any given value of ξ_0, no matter how small it is, using the same numerical method. But for a given computer there is a minimum value of ξ_0 for practical calculations, mainly because of the limitation of the computer storage. Since the general tendency of the change of the solution is consistent as we decrease the value of ξ_0, we can speculate that the modon with extremely small ξ_0 should be like a 'hollow vortex' which has a strong vortex sheet forming its elongated boundary but almost no vorticity inside it.

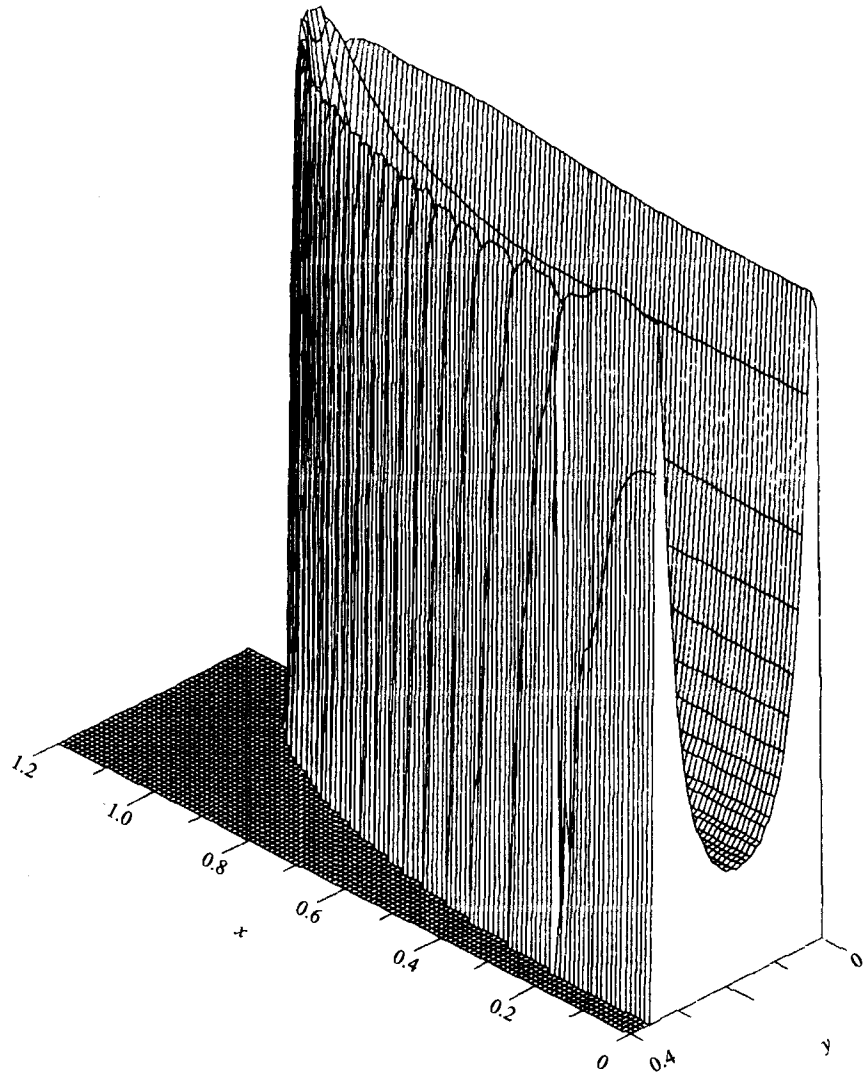

FIGURE 4. Contour plot of vorticity for $\xi_0 = 0.35$.

An interesting discovery in figures 5(*b*) and 5(*c*) is that the curve of vorticity versus streak function bends toward the horizontal axis as the absolute value of the streak function increases. This means that the maximum value of vorticity happens at some moderate value of streak function but not at its extremes. This result is totally different from those of other studies in which the vorticity maximum always corresponds to the maximum value of streak function (McWilliams 1983; Kloosterziel & Van Heijst 1989).

Although we did not impose the condition that vorticity has to be continuous at the boundary, it turns out that for the present numerical modon solution this condition is satisfied automatically, i.e. the vorticity $\zeta = F(\Psi)$ vanishes at the boundary (figure 5*c*). The justification of this result is that $F(\Psi(0,\eta)) = F(\Psi(\xi,0)) = F(\Psi(\xi,\pi)) = 0$ because Ψ and ζ are antisymmetric about $\xi = 0$, $\eta = 0$ and $\eta = \pi$. Because $F(\Psi(\xi,\eta))$ is a single-valued function of Ψ and the boundary ellipse $\xi = \xi_0$ intersects both $\eta = 0$ and $\eta = \pi$, hence $F(\Psi(\xi_0,\eta)) = 0$.

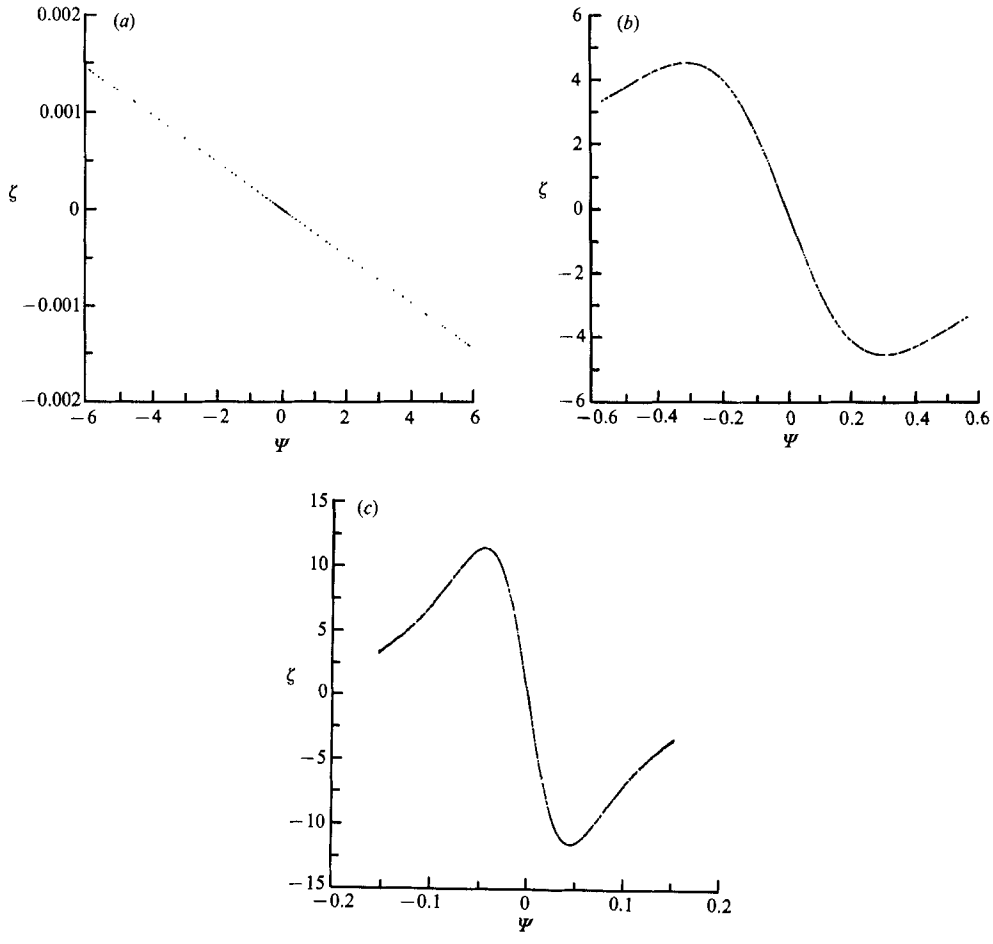

FIGURE 5. Scatter plots of vorticity versus streak function. (*a*) $\xi_0 = 10.0$. (*b*) $\xi_0 = 1.0$. (*c*) $\xi_0 = 0.5$.

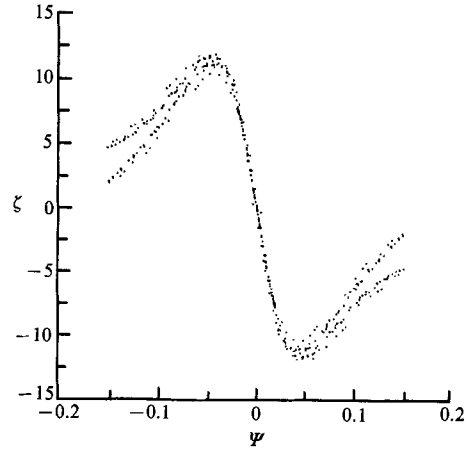

FIGURE 6. Same as figure 5(*c*) but for a smaller basis set. The number of interpolation points in the quasi-radial direction is 25 and that in the angular direction is 8. Because the numerical resolution is too low, the scatter plot shows a great deal of divergence.

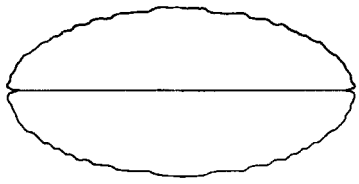

FIGURE 7. Contour plot of vorticity for $\xi_0 = 0.5$ using 80×80 data points. The ripples along the modon boundary are graphing errors, not found in the numerical solution itself.

In order to check the reliability of our results we have repeated each calculation with different numbers of spectral components. We find that when the number of spectral components is small the scatter plot shows a great deal of divergence (figure 6). When we have used enough spectral components, the scatter plot gives a smooth, single-valued curve (figure 5*c*), which helps to demonstrate the correctness of our numerical results. Also as an independent check, we have substituted spectral solutions into the finite difference discretization of (2.2) with a very small grid spacing and confirmed that the residual is very small.

We have obtained some rather confusing pictures when plotting vorticity contours by using standard contouring software (figure 7). The ripples along the modon boundary in figure 7 are artifacts created by the contouring software rather than oscillations in the numerical solution itself. This unrealistic phenomenon can be eliminated by using a ridiculously large number of data points (400×400 data points in a 5 in. $\times$ 5 in. area). We have tried contouring software from several totally different computer resources and surprisingly found that they all inherited the same technical weakness. The problem is that contouring routines approximate the vorticity by piecewise linear interpolation within each square of the contouring grid. Because the vorticity has a discontinuous slope at the vorticity boundary, linear interpolation is a bad approximation whenever the boundary ellipse passes through a contouring square. Buning (1988) catalogues a number of similar (but different) graphical problems.

5. Conclusions and discussion

The present study shows that the two-dimensional modon problem can be solved by the spectral method very efficiently. If the boundary of the modon is elliptical and we require that at least the velocity be continuous, then the relationship between modon streak function and vorticity is nonlinear. The shape of the modon plays an important role in the modon dynamic structure. The maximum vorticity does not appear at the centre of the vortex but near the elliptical modon boundary. Both the maximum vorticity and the intensity of the vorticity gradient near the boundary grow and the vorticity shear is confined in a thinner layer as the eccentricity of the boundary ellipse increases.

Coriolis force and viscosity effects are not considered in the present problem. It would be very interesting to include them in a future study and see what kind of difference they will bring up. There have already been studies about the effect of viscosity in the circular modon case (McWilliams *et al.* 1981), which shows that weak viscosity does not seem to have any significant influence on the basic structure of the solution except that the modon-amplitude slowly decreases with time and smears out the discontinuity of the vorticity slope. We can expect the same thing to happen in the elliptic modon case, too.

The only modification that the Coriolis term will bring about is that the governing equation now is a Helmholtz equation instead of a Laplace's equation, and both the exterior solution and interior solution have to be computed numerically. The numerical method provided in the present paper can still be a powerful tool for these further modon studies.

A number of intriguing questions remain. Why does the function $F(\Psi)$ take the strongly nonlinear shape as it does? Why do the vortices become increasingly 'hollow' and the layers of vorticity thinner as the eccentricity increases? Why does the vorticity concentrate in thin ridges around the edges of each vortex, instead of near the centre? At present we have no physical explanations, even heuristic ones, for these remarkable facts.

This work was supported by the NSF through grants OCE8509923 and OCE8812300 and DMS8716766.

REFERENCES

BATCHELOR, G. K. 1967 *An Introduction to Fluid Dynamics*. Cambridge University Press. 615 pp.

BOYD, J. P. 1985 Equatorial solitary waves. Part 3: Westward-travelling modons. *J. Phys. Oceanogr.* **15**, 46–54.

BOYD, J. P. 1989 *Chebyshev and Fourier Spectral Methods*. Springer. 800 pp.

BUNING, P. G. 1989 Sources of error in the graphical analysis of CDF results. *J. Sci. Comp.* **3**, 149–164.

DEEM, G. S. & ZABUSKY, N. 1978 Stationary 'V-states', interactions, recurrence and breaking. *Solitons in Action* (ed. R. Longren & A. Scott). Academic.

EYDELAND, A. & TURKINGTON, B. 1988 A computational method of solving free boundary problems in vortex dynamics. *J. Comp. Phys.* **78**, 194–214.

FLIERL, G. R., LARICHEV, V. D., MCWILLIAMS, J. C. & REZNIK, G. M. 1980 The dynamics of barotropic and baroclinic solitary waves. *Dyn. Atmos. Oceans* **5**, 1–41.

FLIERL, G. R., STERN, M. E. & WHITEHEAD, J. A. 1983 The physical significance of modons: laboratory experiments and general integral constraints. *Dyn. Atmos. Oceans* **7**, 233–263.

KLOOSTERZIEL, R. C. & VAN HEIJST, G. J. F. 1989 On tripolar vortices. In *Mesoscale/synoptic coherent structures in geophysical turbulence* (ed. J. C. J. Nihoul & B. M. Jamart), pp. 609–626. Elsevier.

LAMB, H. 1932 *Hydrodynamics*. Cambridge University Press.

LARICHEV, V. D. & REZNIK, G. M. 1976 Strongly nonlinear two dimensional solitary Rossby waves. *Oceanologia* **16**, 961–967

LARICHEV, V. D. & REZNIK, G. M. 1983 On collisions between two-dimensional solitary Rossby waves. *Oceanology* **23** (5), 545–552.

MCWILLIAMS, J. C. 1980 An application of equivalent modons to atmospheric blocking. *Dyn. Atmos. Oceanogr.* **5**, 43–66.

MCWILLIAMS, J. C. 1983 Interactions of isolated vortices. II. Modon generation by monopole collision. *Geophys. Astrophys. Fluid Dyn.* **24**, 1–22.

MCWILLIAMS, J. C., FLIERL, G. R., LARICHEV, V. D. & REZNIK, G. M. 1981 Numerical studies of barotropic modons. *Dyn. Atmos. Oceans* **5**, 219–238.

MCWILLIAMS, J. C. & ZABUSKY, N. J. 1982 Interactions of isolated vortices. I. Modons colliding with modons. *Geophys. Astrophys. Fluid Dyn.* **19**, 207–227.

MALANOTTE-RIZZOLI, P. 1982 Planetary solitary waves in geophysical flows. *Adv. Geophys.* **24**, 147–221.

PIERREHUMBERT, R. T. 1980 A family of steady translation vortex pairs with disturbed vorticity. *J. Fluid Mech.* **99**, 129–144 and corrigendum 1981, **102**, 478.

SHEN, C. Y. 1981 On the dynamics of a solitary vortex. *Dyn. Atmos. Oceans* **5**, 239–267.

STERN, M. E. 1975 Minimal properties of planetary eddies. *J. Mar. Res.* **33**, 1–13.

TANVEER, S. 1986 A steadily translating pair of equal and opposite vortices with vortex sheets on their boundaries. *Stud. Appl. Maths* **74**, 139–154.

TRIBBIA, J. J. 1984 Modons in spherical geometry. *Geophys. Astrophys. Fluid Dyn.* **30**, 131–168.

VERKLEY, W. 1984 The construction of barotropic modons on a sphere. *J. Atmos. Sci.* **41**, 2492–2504.

VERKLEY, W. 1987 Stationary barotropic modons in westerly background flows. *J. Atmos. Sci.* **44**, 2383–2398.